International Journal of Modern Physics B
© World Scientific Publishing Company

EXACT AND SELF-CONSISTENT RESULTS IN ONE-DIMENSIONAL REPULSIVE HUBBARD MODEL

Armen N. Kocharian

Department of Physics and Astronomy, California State University, Northridge, CA 91330-8268, U.S.A.
armen.n.kocharian@csun.edu

C. Yang

Department of Physics, Tamkang University, Tamsui, Taiwan 251
cyang@mail.tku.edu.tw

Y. L. Chiang

Department of Physics, Chinese Culture University, Taipei, Taiwan 111
yuling@faculty.pccu.edu.tw

T. Y. Chou

Department of Physics, National Chung Cheng University Chia-Yi, Taiwan 621

Received (June 2003)

The shortcomings and advantages of the generalized self-consistent field (GSCF) approach, which includes the electron-hole order parameter $\Delta_q^{(+)}$ and the average spin s within the one-dimensional repulsive Hubbard model, are analyzed by comparison of the ground state properties with the corresponding Bethe-*ansatz* results in an entire parameter space of interaction strength $U/t \geq 0$, magnetic field $h \geq 0$ and electron concentration $0 \leq n \leq 1$. The GSCF spectral characteristics are derived and criteria are found for the stability of incommensurate magnetic phase with the wave number $0 < q < \pi$. The GSCF theory displays a simple relationship for the double occupancy $D^{(+)}$ in terms of n, s and $\Delta_q^{(+)}$, where $D^{(+)}$ underestimates electron correlations at weak and intermediate ranges and overestimates correlations at large interaction strengths. Beyond some critical U/t and $n \neq 1$ the GSCF $D^{(+)}$ for spatially homogeneous state vanishes, while the exact D for all n at $h = 0$ decreases gradually as U/t increases. At $n \neq 1$ the GSCF chemical potential $\mu^{(+)}$ overestimates electron correlations everywhere and variation $\mu^{(+)}$ *versus* n displays electron instability toward the phase separation in the vicinity of $n = 1$. Exactly at $n = 1$ the GSCF $\mu^{(+)}$ *versus* U/t always underestimates electron correlation and as $U/t \to \infty$ at $h = 0$ we have $\mu^{(+)} \to 0$, while the Bethe-*ansatz* result gives $\mu \to 2t$. In the limiting cases $U/t \to 0$ and $U/t \to \infty$ for all $h \geq 0$ and $0 \leq n \leq 1$ the GSCF ground state energy is exact, which is necessary for formulation of converging perturbation procedure about mean field solution in the entire parameter space.

Keywords: Hubbard model, Bethe-*ansatz*, mean field, electron instability, correlation.

1. Motivation

There are still open questions and unresolved problems with regards to the understanding of the metallic ferro- and antiferromagnetism even for the minimal Hubbard model with few adjustable parameters. This model received renewed attention with the discovery of self-organized stripes in the high-T_c superconductors (HTSC).[1–2] It is also a prototypical model for the studies of non-Fermi liquid behavior in quasi-one dimensional metals;[3] the phase-separated states in doped cuprates and lanthanum-based manganites;[4] unusual ferromagnetism in half metallic magnets;[5,6] the magnetism of organic and inorganic quasi-one dimensional magnetic conductors, insulators and superconductors.[7–10]

Much progress has been achieved in the understanding of many body electron correlations in infinite and finite 2d lattices, using mean-field,[11–14] slave bosons,[15]random phase approximations (RPA),[16] exact diagonalization and quantum Monte-Carlo (QMC) calculations.[17–20] Among the different methods, surprisingly insufficient attention was given to the detailed analysis of standard mean field approximation, which often allows to formulate a problem in physically transparent way and get analytical solution in any spatial dimension (d).[21,22] However, nonperturbed mean field scheme is difficult to justify since there is no small parameter, and its predictions are sometimes washed out in more accurate calculations.[23]

For evaluation of mean field theory and development of more accurate RPA-type perturbation techniques by including the fluctuations about mean field solution it is necessary systematic numerical studies of mean field ground state properties.[24] It is the lack of the exact solution in the thermodynamic limit in 2d case that puts the test of the most general linear mean field theory, using the Bethe-*ansatz* theory,[25–33] on a firmer basis in the extreme conditions of one dimensionality.[14,34,35]

Due to strong quantum disorder the universal mean-field scheme with continuous broken symmetry is traditionally considered inadequate for strongly correlated systems in 1d case. It is certainly true for long-range characteristics, while short-range correlations can address some ground state properties quantitatively correct in wide range of $U > 0$ and $U < 0$ Hubbard model even in 1d case.[13,29,36]

In the present paper we compare the Bethe-ansatz and generalized self-consistent field (GSCF) ground state properties in the entire parameter space of U/t, magnetic field h and electron concentration n. Our developed GSCF approach is a straightforward extension of existing mean-field solutions for general U/t, n and h.[36,37–38]

Many authors have discussed the opportunity of the phase separation instability within the s-d, Hubbard and t-J models.[4,39,40–42] The recent interest to the phase separation in the HTSC materials[1–3] made us undertake a detailed examination of this feature within the GSCF approximation. We show that the GSCF chemical potential within a certain range of parameters, U/t and n displays electron instability, while the Bethe-*ansatz* gives stable monotonous solution everywhere.

The GSCF U/t-n phase diagram shows the tendency toward the spin saturation, ferro-, antiferro- and spiral (incommensurate) ordering as in higher

dimensions,[11,19,36,43] although the exact ground state for 1d system at $h = 0$ is a singlet.[44] However, in contrast to the 2d case [38] the GSCF paramagnetic in the 1d case energetically unstable at all $n \neq 1$ no matter how small U/t is.

Exactly at half-filling we studied the electron-hole (exciton) BCS-like pairing and magnetic crossover from itinerant into Bose-Einstein condensation regime driven by U/t and h.[45] In the Mott-Hubbard insulator, the quasi-particle energy gap undergoes transformation in the momentum space and the GSCF theory predict on the way to the saturated phase a certain distinction between the magnetic ordering with well-developed (*localized*) moments and weak band-like (*itinerant*) magnetism.

Finally, we show that the GSCF variational energy for arbitrary $h \geq 0$ and $0 \leq n \leq 1$ is exact in both limiting cases $U/t \to 0$ and $U/t \to \infty$. This substantial input allows to formulate more accurate and rigorous perturbation procedure about mean field solution, which can establish the relationship for general U/t, h and n between the converging perturbation theory and variational principle.[24]

The paper is organized as follows. After the introduction, we present the GSCF formalism in section 2. In sections 3 and 4 we study ground-state properties, spectral characteristics, and phase diagram by incorporating various magnetic structures. In section 5 we provide the detailed description of the magnetic crossover from the itinerant into localized magnetism. The concluding summary constitutes Section 6. In Appendixes we examine the GSCF quasi-particle spectrum at weak interaction limit and derive the Bethe-ansatz ground state properties.

2. GSCF formalism

2.1. *Decoupling scheme*

We consider the repulsive Hubbard Hamiltonian ($U > 0$) with magnetic field ($h \geq 0$)

$$H_h = -t \sum_{\langle i,\, j\rangle,\, \sigma} c^+_{i\sigma} c_{j\sigma} + U \sum_i c^+_{i\uparrow} c^+_{i\downarrow} c_{i\downarrow} c_{i\uparrow} - \frac{h}{2} \sum_i \left(c^+_{i\uparrow} c_{i\uparrow} - c^+_{i\downarrow} c_{i\downarrow} \right). \tag{1}$$

According to the Wick theorem (see, *e. g.* Ref. 46, p. 362-363) the following single-particle decoupling is assumed for interaction term in (1)

$$\begin{aligned} c^+_{j\uparrow} c^+_{j\downarrow} c_{j\downarrow} c_{j\uparrow} \approx {} & \langle c^+_{j\uparrow} c_{j\uparrow} \rangle c^+_{j\downarrow} c_{j\downarrow} + \langle c^+_{j\downarrow} c_{j\downarrow} \rangle c^+_{j\uparrow} c_{j\uparrow} - \langle c^+_{j\uparrow} c_{j\uparrow} \rangle \langle c^+_{j\downarrow} c_{j\downarrow} \rangle \\ & - \langle c^+_{j\uparrow} c_{j\downarrow} \rangle c^+_{j\downarrow} c_{j\uparrow} - \langle c^+_{j\downarrow} c_{j\uparrow} \rangle c^+_{j\uparrow} c_{j\downarrow} + \langle c^+_{j\uparrow} c_{j\downarrow} \rangle \langle c^+_{j\downarrow} c_{j\uparrow} \rangle. \end{aligned} \tag{2}$$

The approximation (2) takes into account the effect of electron-electron and electron-hole interaction in a linear approximation as an average single-particle (mean field) terms. The average local electron numbers $n^c_{j\sigma} \equiv \langle c^+_{j\sigma} c_{j\sigma} \rangle$ or corresponding concentration of electrons and average spin are

$$\begin{aligned} n \equiv \langle \hat{n} \rangle &\equiv \frac{1}{N_{\rm latt}} \sum_j \left\langle c^+_{j\uparrow} c_{j\uparrow} + c^+_{j\downarrow} c_{j\downarrow} \right\rangle, \\ s \equiv \langle \hat{S}_z \rangle &\equiv \frac{1}{2N_{\rm latt}} \sum_j \left\langle c^+_{j\uparrow} c_{j\uparrow} - c^+_{j\downarrow} c_{j\downarrow} \right\rangle. \end{aligned} \tag{3}$$

The introduced local electron-hole order parameter $\Delta_j^{(+)} \equiv \langle c_{j\uparrow}^+ c_{j\downarrow} \rangle$ is connected with $\Delta_{\mathbf{q}}^{(+)} \equiv -(2U/N_{\rm latt}) \sum_{\mathbf{k}} \langle c_{\mathbf{k}\uparrow}^+ c_{\mathbf{k}+\mathbf{q}\downarrow} \rangle$

$$\Delta_j^{(+)} = -\frac{\Delta_{\mathbf{q}}^{(+)}}{2U} \exp i(\mathbf{q} \cdot \mathbf{r}_j). \tag{4}$$

The average $\Delta_j^{(-)} \equiv \langle c_{j\uparrow} c_{j\downarrow} \rangle$ in (2) for $U > 0$ is neglected. Here and below the superscripts "$(\pm)$" signify solutions for $U > 0$ and $U < 0$ respectively.

We consider the homogeneous spatial distribution of electron density and put $n_\sigma^c = n_{j\sigma}^c$ independently of the lattice site. The solution with the total momentum of the center of mass $\mathbf{q} \neq 0$ for the electron-hole pair corresponds to the spatially inhomogeneous spiral spin density waves (see section 3.1). We call this approach developed for arbitrary $U \geq 0$, $h \geq 0$ and all $0 \leq n \leq 1$ as generalized self-consistent field (GSCF) approximation.

In the GSCF approach according to (2) the concentration of double occupied sites $D^{(+)}$ can be reduced to a simple expression

$$D^{(+)} \equiv \frac{1}{N_{\rm latt}} \sum_j \langle c_{j\uparrow}^+ c_{j\downarrow}^+ c_{j\downarrow} c_{j\uparrow} \rangle = D_0 - \frac{(\Delta_{\mathbf{q}}^{(+)})^2}{4U^2}, \tag{5}$$

valid for arbitrary U/t, n and s. Here $D_0 \equiv n^2/4 - s^2$ is the limiting value of $D^{(+)}$ for all U/t, n and s while $\Delta_{\mathbf{q}}^{(+)} = 0$. The magnitude $D^{(+)}$ in (5) depends on $\mathbf{q}$ and decreases in expense of the density of bound electron-hole pairs $(\Delta_{\mathbf{q}}^{(+)})^2/4U^2$.

2.2. *Canonical transformation*

Using the standard Bogoliubov canonical transformation to the new Fermi quasi-particle operators

$$\begin{aligned} \alpha_{\mathbf{kq}+}^+ &= w_{\mathbf{kq}} c_{\mathbf{k}\uparrow}^+ + y_{\mathbf{kq}} c_{\mathbf{k}+\mathbf{q}\downarrow}^+, \\ \alpha_{\mathbf{kq}-}^+ &= y_{\mathbf{kq}} c_{\mathbf{k}\uparrow}^+ - w_{\mathbf{kq}} c_{\mathbf{k}+\mathbf{q}\downarrow}^+ \end{aligned} \tag{6}$$

($w_{\mathbf{kq}}^2 + y_{\mathbf{kq}}^2 = 1$) the single-particle (quadratic) Hamiltonian $H_{\rm GSCF}^{(+)}$ in the GSCF approach (2) is diagonalized and the average energy $E_h^{(+)} \equiv \langle H_{\rm GSCF}^{(+)} \rangle$ is reduced to

$$E_h^{(+)} = \frac{1}{N_{\rm latt}} \sum_{\mathbf{k},\lambda} \mathcal{E}_{\mathbf{k}\lambda}^{(+)}(\mathbf{q}) n_{\mathbf{kq}\lambda}^{(+)} - UD^{(+)}, \tag{7}$$

where $n_{\mathbf{kq}\lambda}^{(+)}$ are the occupation numbers of the quasi-particle states

$$n_{\mathbf{kq}\lambda}^{(+)} \equiv \langle \alpha_{\mathbf{kq}\lambda}^+ \alpha_{\mathbf{kq}\lambda} \rangle = 1 \text{ (if } \mathbf{k} \in \mathcal{K}_{\rm F}) \quad \text{or} \quad 0 \text{ (if } \mathbf{k} \notin \mathcal{K}_{\rm F}), \tag{8}$$

and $\mathcal{K}_{\rm F}$ is the Fermi region (do not mix $n_{\mathbf{kq}\lambda}^{(+)}$ with the electron occupation number $n_{\mathbf{k}\sigma}^c \equiv \langle c_{\mathbf{k}\sigma}^+ c_{\mathbf{k}\sigma} \rangle$). Indexes $\lambda = \pm$ in (7) denote the two quasi-particle states and differ from electron spin states σ. The two quasi-particle sub-bands in (7) are

$$\mathcal{E}_{\mathbf{k}\lambda}^{(+)}(\mathbf{q}) = \frac{\epsilon_{\mathbf{k}} + \epsilon_{\mathbf{k}+\mathbf{q}} + nU}{2} - \lambda E_{\mathbf{k}}^{(+)}(\mathbf{q}), \tag{9}$$

where the dispersion relation for electrons is

$$\epsilon_{\mathbf{k}} = -2t\cos\left(\mathbf{k}\cdot\mathbf{R}\right) \tag{10}$$

with $\mathbf{R} \equiv \mathbf{r}_{j+1} - \mathbf{r}_j$. The energy difference between these sub-bands is

$$2E_{\mathbf{k}}^{(+)}(\mathbf{q}) = \sqrt{(\epsilon_{\mathbf{k}} - \epsilon_{\mathbf{k}+\mathbf{q}} - 2Us - h)^2 + \left(\Delta_{\mathbf{q}}^{(+)}\right)^2}\,. \tag{11}$$

2.3. *Self-consistent equations*

In equilibrium the minimization of energy $E_h^{(+)}$ with respect to s, $\Delta_q^{(+)}$ and q in 1d case gives the following system of nonlinear self-consistent equations

$$2s + \frac{1}{2N_{\rm latt}}\sum_k \frac{\epsilon_k - \epsilon_{k+q} - 2sU - h}{E_k^{(+)}(q)}\left(n_{kq+}^{(+)} - n_{kq-}^{(+)}\right) = 0, \tag{12}$$

$$\Delta_q^{(+)}\left(1 - \frac{U}{2N_{\rm latt}}\sum_k \frac{n_{kq+}^{(+)} - n_{kq-}^{(+)}}{E_k^{(+)}(q)}\right) = 0, \tag{13}$$

$$\sum_k \sin(k+q)\left(n_{kq+}^{(+)} + n_{kq-}^{(+)} + \frac{(\epsilon_k - \epsilon_{k+q} - 2Us - h)(n_{kq+}^{(+)} - n_{kq-}^{(+)})}{2E_k^{(+)}(q)}\right) = 0. \tag{14}$$

We must add also the normalization condition to assure the conservation of the number of quasi-particles

$$\frac{1}{N_{\rm latt}}\sum_k \left(n_{kq+}^{(+)} + n_{kq-}^{(+)}\right) = n = n_\uparrow^c + n_\downarrow^c. \tag{15}$$

We consider $n \leq 1$, while $n \geq 1$ can be treated similarly due to electron-hole symmetry.

3. Spin (magnetic) structure

3.1. *Local moment and lattice moment*

The spin operators

$$\hat{s}_{jx} \equiv \frac{1}{2}\left(c_{j\uparrow}^+ c_{j\downarrow} + c_{j\downarrow}^+ c_{j\uparrow}\right), \qquad \hat{s}_{jy} \equiv \frac{1}{2i}\left(c_{j\uparrow}^+ c_{j\downarrow} - c_{j\downarrow}^+ c_{j\uparrow}\right),$$
$$\hat{s}_{jz} \equiv \frac{1}{2}\left(c_{j\uparrow}^+ c_{j\uparrow} - c_{j\downarrow}^+ c_{j\downarrow}\right) \tag{16}$$

satisfy the usual commutation relations. Averaging over all lattice sites j gives the lattice spin components $\hat{S}_x, \hat{S}_y, \hat{S}_z$. There are direct relationships between the expectation values for the local spin components $\langle\hat{s}_{jx}\rangle$, $\langle\hat{s}_{jy}\rangle$, $\langle\hat{s}_{jz}\rangle$ and the parameters $n_\uparrow^c$, $n_\downarrow^c$, $\Delta_j^{(+)}$. Namely,

$$\langle\hat{s}_{jx}\rangle = {\rm Re}\Delta_j^{(+)}, \quad \langle\hat{s}_{jy}\rangle = {\rm Im}\Delta_j^{(+)}, \quad \langle\hat{s}_{jz}\rangle = s = \frac{1}{2}(n_\uparrow^c - n_\downarrow^c), \tag{17}$$

where the transverse local spin $s_{j\perp} = |\Delta_j^{(+)}|$ components are modulated by a wave number q (see (4))

$$\langle \hat{s}_{jx} \rangle = -\frac{\Delta_q^{(+)}}{2U} \cos(qj), \quad \langle \hat{s}_{jy} \rangle = -\frac{\Delta_q^{(+)}}{2U} \sin(qj). \tag{18}$$

Taking into account (18), for the average transverse lattice spin $S_\perp \equiv (\langle \hat{S}_x \rangle^2 + \langle \hat{S}_y \rangle^2)^{1/2}$ we get

$$S_\perp = 0 \quad \text{if} \quad q \neq 0, \tag{19}$$

$$S_\perp = \frac{|\Delta_0^{(+)}|}{2U} \quad \text{if} \quad q = 0. \tag{20}$$

The expectation value of the lattice spin component along the magnetic field is a longitudinal magnetization s. The solution with $q \neq 0$ describes a spatially inhomogeneous state, while at $h = 0$ the uniform state with $q = 0$ may be conditionally called as the "transverse ferromagnetic" one ($s = 0$, $S_\perp = n/2$). This state has the same energy as that of the fully polarized ferromagnetic state ($s = n/2$, $S_\perp = 0$, q is arbitrary) at the same U/t and n in the presence of infinitesimal magnetic field $h \to 0$ (sections 3.3 and 4.5). A "transverse spiral incommensurate" phase with $0 < q < \pi$ exists only at $n \neq 1$ (see below) as in higher dimensions.[37,38,36] The spin of conduction electron feels the spatially varying effective spins of other electrons (18) similar to the spiral phase in the Kondo model.[52]

3.2. *Limiting cases*

The limiting ground-state energy at $U \to 0$ is[35]

$$E_h^{(+)} = -\frac{4t}{\pi} \sin\left(\frac{n\pi}{2}\right) \cos(s\pi) - hs, \tag{21}$$

$$s = \begin{cases} \dfrac{1}{\pi} \arcsin \dfrac{h}{4t \sin(n\pi/2)} & \text{for } 0 \leq h \leq h_{\rm sat}, \\ n/2 & \text{for } h_{\rm sat} < h, \end{cases} \tag{22}$$

where $h_{\rm sat}$ (or $h_{\rm c2}$ in [35]) is the critical field for the longitudinal spin saturation[50] at $U/t \to 0$

$$h_{\rm sat} = 2t(1 - \cos n\pi). \tag{23}$$

At weak interaction limit we have also

$$\lim_{U/t \to +0} \Delta_q^{(+)} = 0, \qquad \lim_{U/t \to +0} q = n\pi, \tag{24}$$

independently of h/t. The GSCF relation for the wave number $q = \pi n$ at $U/t \ll 1$ is consistent with the exact result for the lattice momentum q in two-particle correlation function.[36,56,57]

At large $U/t \gg 1$ limit from the GSCF approach we find

$$\lim_{U/t \to \infty} s = 0, \qquad \lim_{U/t \to \infty} S_\perp = \frac{n}{2}, \tag{25}$$

at $h = 0$ and correspondingly

$$\lim_{U/t\to\infty} s = \frac{n}{2}, \qquad \lim_{U/t\to\infty} S_\perp = 0 \tag{26}$$

at $h \neq 0$. For the GSCF approach q is zero (at $n \neq 1$) in (25) or becomes arbitrary (at arbitrary n) in (26).

In the exact theory at $h = 0$ the transverse spin never becomes saturated no matter how strong is U/t or how small is $n \neq 0$. Also at low density limit the problem is simplified significantly in any dimension[47] and for an empty band we find that the GSCF ground state properties coincide with corresponding Bethe-ansatz results for general U/t and h. Indeed, at $n \to 0$ both results are the same: $E^{(+)} \to 0$, $D^{(+)} \to 0$ and $\mu^{(+)} \to -2t - h/2$, independently of U/t.[35,48]

3.3. *Order parameter* $\boldsymbol{\Delta_q^{(+)}}$

The order parameter $\Delta_q^{(+)}$ and the average spin s both are continuous functions of U/t, n, and h (figure 1). From equation (5) we obtain a simple relationship between $|\Delta_q^{(+)}|$ and $D^{(+)}$:

$$|\Delta_q^{(+)}| = 2U\sqrt{D_0 - D^{(+)}}, \tag{27}$$

valid in the entire space of U/t, n and s values.

The order parameter $|\Delta_q^{(+)}|$ does not have corresponding analogue in the exact theory. However we can compare $|\Delta_q^{(+)}|$ with analogous parameter $|\Delta_{\rm ex}^{(+)}| \equiv 2U\sqrt{D_0 - D}$, using the Bethe-*ansatz* result for D (C.1) (Appendix C).

In figure 1 at $h = 0$ we have $s = 0$, while $|\Delta_q^{(+)}|/2U$ increases monotonously with U/t and becomes saturated (if $n < 1$) as U exceeds some $U_{\rm homog}$ (marked by rhombuses). At $h = 0$ and $n = 1$ we have $|\Delta_q^{(+)}|/2U \to 1/2$ at $U/t \to \infty$. At $h > 0$ the spin s increases with U/t and becomes saturated ($s = n/2$) as U exceeds $U_{\rm sat}$ (marked by downward-pointing triangles), while $|\Delta_q^{(+)}|/2U$ vanishes at $U \geq U_{\rm sat}$.

The GSCF results (dashed curves) qualitatively agree with the exact ones (solid curves) at large U/t and strong field h. Our calculations show that the total spin

$$S_{\rm tot} \equiv (s^2 + S_\perp^2)^{1/2} \tag{28}$$

monotonously increases with U/t and h as in the exact theory.

In general, the behavior of wave number q *versus* U/t and n (figures 2 and 3) in 1d case qualitatively resembles the corresponding one obtained for a square lattice.[36] In fact, the parameter q linearly increases with electron concentration in some range of U/t and exactly at $n = 1$ it is independent of U/t (figure 3). However, at $h = 0$ and $n < 1$ the GSCF ground state is an incommensutrate phase, while paramagnetic phase is a more stable mean field solution in higher dimensions.[38,17] As in higher dimensions, there is a GSCF uniform solution $S_\perp = |\Delta_0^{(+)}|/2U$ with $q = 0$, and maximum transverse magnetization (25) is stable at $h = 0$ and larger $U \geq U_{\rm homog}$ (figure 2 and 3). Also the GSCF solution (26) in the presence of magnetic field

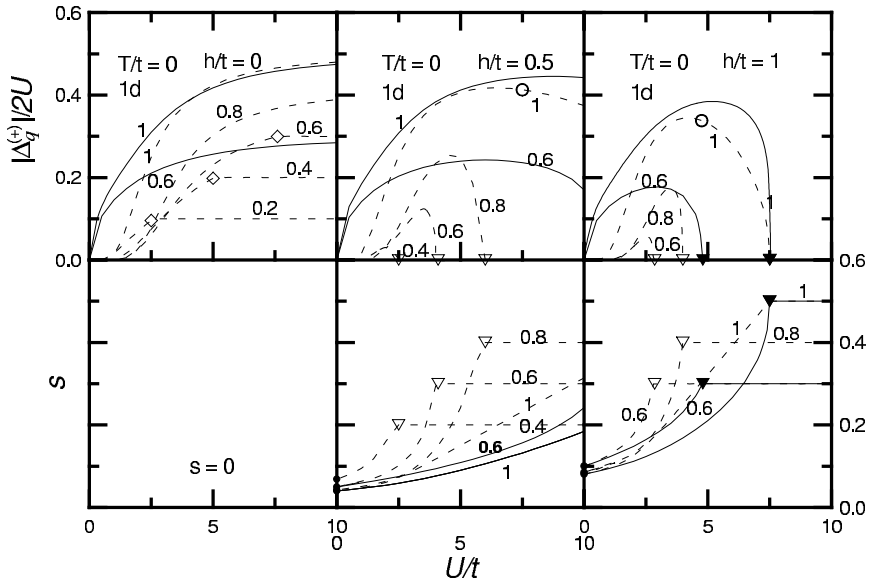

Fig. 1. The ground-state longitudinal (s) and the local transverse ($|\Delta_q^{(+)}|/2U$) spin components as a function of U/t for various n (figures label the curves) and h in the GSCF approach (dashed curves) along with the one-dimensional Bethe-*ansatz* result for $n = 1$ and $n = 0.6$ (solid curves). The triangles and rhombuses mark the longitudinal and transverse spin saturation correspondingly.

becomes fully saturated ($s = n/2$) and degenerate ($|\Delta_q^{(+)}|/2U = 0$ with q arbitrary) at $U \geq U_{\rm sat}$ (on the right of triangles in figures 1 and 2) or $n < n_{\rm sat}$ (on the left of the triangles in figure 3).

Even though at $h \neq 0$ there is no true long-range order in 1d case, by comparison of the GSCF quasi-particle spectrum, ground-state properties and the phase diagram to the exact results we can estimate the short range electron correlations (sections 4.1–4.5).

4. Ground-state properties

4.1. *Quasi-particle spectrum*

In the common case of $0 \leq n < 1$ the situation $\min\{\mathcal{E}_{k-}^{(+)}(q)\} < \max\{\mathcal{E}_{k+}^{(+)}(q)\}$ may occur. But we never found the case when the Fermi-energy was higher than the minimum of the upper band, *i. e.* the corresponding upper band is always empty for all U/t, h and $n \neq 1$. The corresponding energy gap (see (9)) at $n = 1$ for the quasi particle-hole excitations is $E_{\rm gap}^{(+)} = 2\min\{E_{\mathbf{k}}^{(+)}(\pi)\}$ (figure 4).

At all n there is a correlation in the position of the minimum energy difference (11) between the two sub-bands and the wave number q shown by rhombuses in figure 5. As figure 4 and figure 5 make it apparent, at arbitrary U electron-hole correlations remove the Kramers degeneracy, so that the quasi-particles near half-

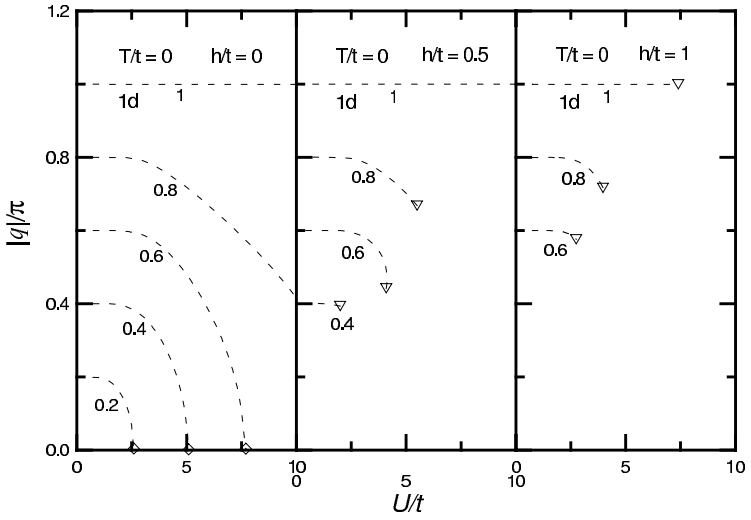

Fig. 2. The GSCF optimized wave number q of local transverse spin modulation as a function of U/t for various n (figures label the curves) and h/t. The triangles and rhombuses mean the same as in figure 1.

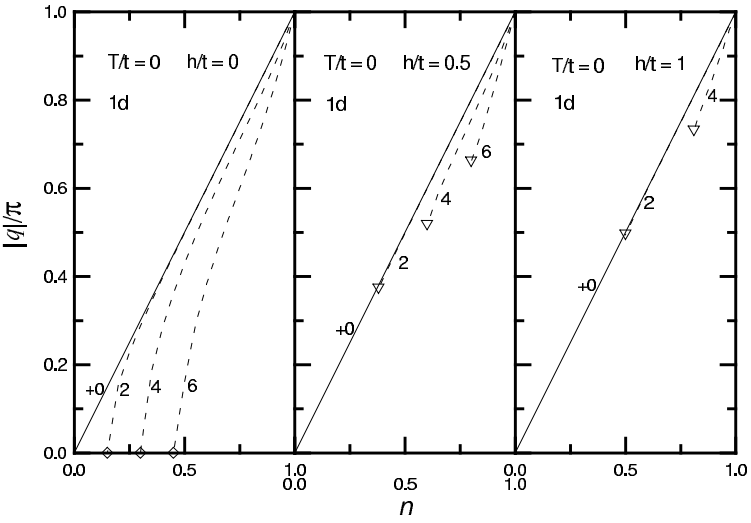

Fig. 3. q as a function of n for various U/t (figures label the curves) and h/t. The triangles and rhombuses mean the same as in figure 1.

filling fill the "anomalous" large region in the momentum space ($k \in \mathcal{K}_{\mathrm{F}}$). In both figures the occupied Fermi region is shown by thick curves.

Although in many cases there are only two Fermi-impulses (k_{F1}, k_{F2}) corre-

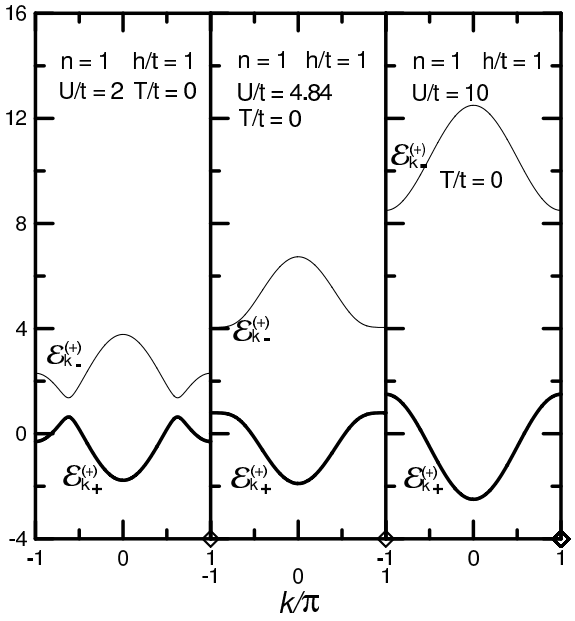

Fig. 4. The GSCF quasi-particle energy spectrum (9) for $n = 1$, $h/t = 1$. The critical interaction strength for the longitudinal spin saturation $U_{\rm sat}/t = 7.5$. The thick curves correspond to the occupied parts of the single quasi-particle states in the momentum space. In the represented cases $s = 0.13,\ 0.31,\ 0.50$; $|\Delta_\pi^{(+)}|/t = 0.73,\ 3.25,\ 0.05$; $D^{(+)} = 0.20,\ 0.04,\ 0$; $h + 2Us - 4t = -2.48,\ 10^{-4},\ 7$ correspondingly. The rhombuses note q in (9).

sponding to the same Fermi energy $E_{\rm F}$, in some cases we found at $h \neq 0$ also more than the two Fermi-impulses ($k_{\rm F1}$, $k_{\rm F2}$, $k_{\rm F3}$, $k_{\rm F4}, \ldots$). In general the occupied part of the k-space within the first Brillouin zone happens to be closed or open, symmetric or non-symmetric with respect to the origin of the k-space (figure 5). Thus it is more convenient to simply introduce the width of the occupied part in the momentum space ($k \in \mathcal{K}_{\rm F}$)

$$W_{\rm Fermi} \equiv (k_{\rm F2} - k_{\rm F1}) + (k_{\rm F4} - k_{\rm F3}) + \cdots . \tag{29}$$

At $n \leq 1$ the width of the occupied region in the lower band $W_{\rm Fermi} = n\pi$ according to (15) and is independent from U/t and h/t. This result is consistent with the Luttinger theorem.[55,56]

In the limit $U/t \to 0$ and $n \leq 1$ the quasi-particles $n_{kq+}^{(+)}$ occupy Fermi region in the k-space between the Fermi-points $k_{\rm F1} \leq k \leq k_{\rm F2}$ symmetric with respect to k_0 (see Appendix A), where $k_0 = 0$ at $n = 1$. Below we compare the GSCF and exact ground state properties in the entire space of U/t, $h \geq 0$ and $0 \leq n \leq 1$.

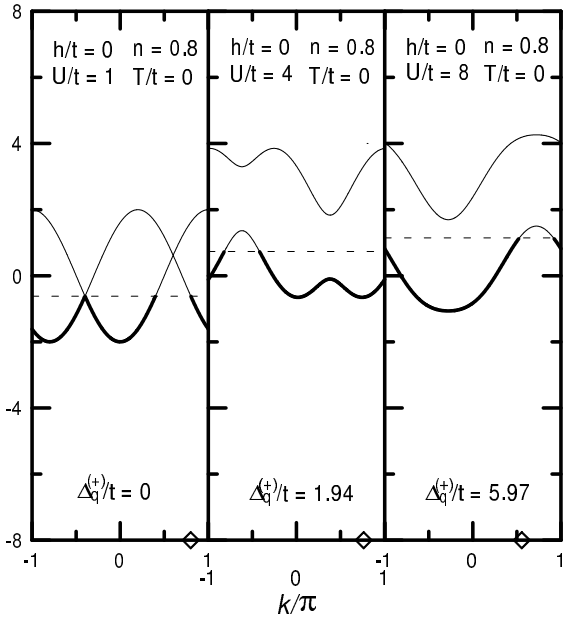

Fig. 5. The GSCF quasi-particle energy spectrum (9) for $n = 0.8$, $h/t = 0$ and $U/t = 1.0, 4.0, 8.0$. The notation is the same as for figure 4. In the represented cases $s = 0$; $|\Delta_\pi^{(+)}|/t = 0.00,\ 1.94,\ 5.97$; $D^{(+)} = 0.16,\ 0.10,\ 0.02$, correspondingly. The Fermi regions are open and non-symmetric with respect to $k = 0$.

4.2. *Total energy*

First we calculated the ground state energy in the GSCF approach and in the exact theory (see Appendix B).

In figure 6 both results are shown as functions of U/t for various h and n. The total energy increases (algebraically) with U/t (figure 6). The GSCF energy calculated by means of (7) coincides with the Bethe-*ansatz* result in the limiting cases $U/t \to 0$ and $U/t \to \infty$ for all h and n and these results agree with each other quite well in the entire range of U/t, $h \geq 0$ and $0 \leq n \leq 1$.

4.3. *Chemical potential*

In figures 7 and 8 the Bethe-*ansatz* results (Appendix B) of μ *versus* U/t and n at given h/t (the solid curves) are compared with the GSCF ones (the dashed curves). The exact μ is a monotonous and smooth function of U/t, n and h except the sharp kinks at the critical interaction strengths $U_{\rm sat}$ (triangles in figure 8) or at the critical electron concentrations $n_{\rm sat}$ (triangles in figure 8).

In contrast the GSCF $\mu^{(+)}$ is non-monotonous in some range of U/t , n and h (figures 7 and 8). The variation of $\mu^{(+)}$ *versus* U/t in figure 7 shows monotonous behavior for all $n \neq 1$ and as in exact theory $\mu^{(+)}$ at weak interaction increases

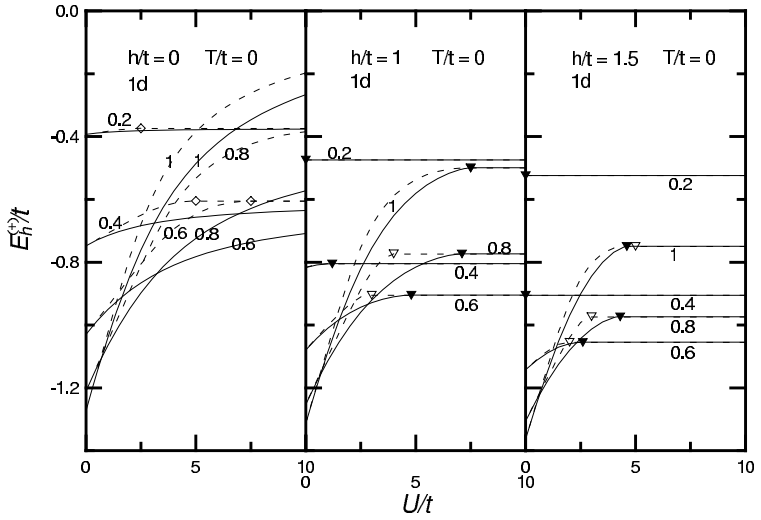

Fig. 6. The ground state energy $E_h^{(+)}$ as a function of U/t for various n and h/t. The notation is the same as for figure 1. The solid triangles mean the same as in figure 1.

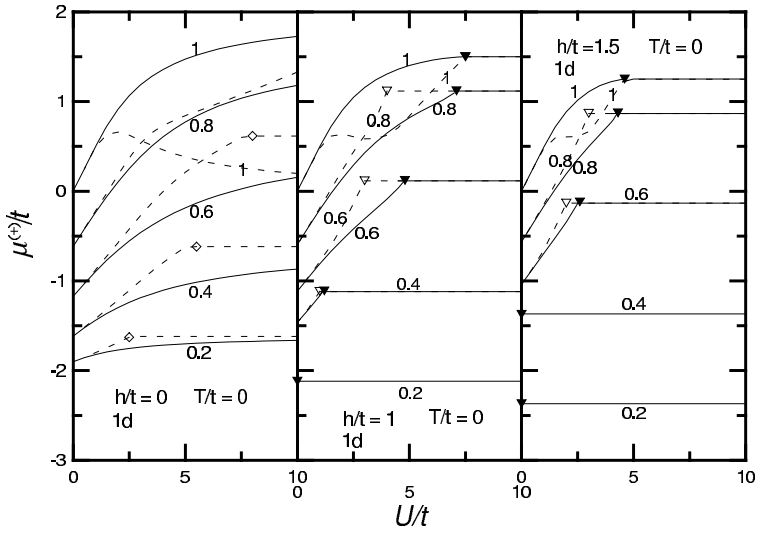

Fig. 7. The ground state chemical potential $\mu^{(+)}$ as a function of U/t for various n and h/t. The notation is the same as for figure 1.

with $U/t \ll 1$ linearly. Also, except $n = 1$ case, the numerical agreement between $\mu^{(+)}$ and μ becomes more accurate with increasing U/t. For $n \neq 1$ the GSCF result for $\mu^{(+)}$ everywhere slightly overestimates electron correlations (figure 7). But $\mu^{(+)}$ at $n = 1$ is non-monotonous in intermediate region of U/t and as $U/t \to \infty$ and

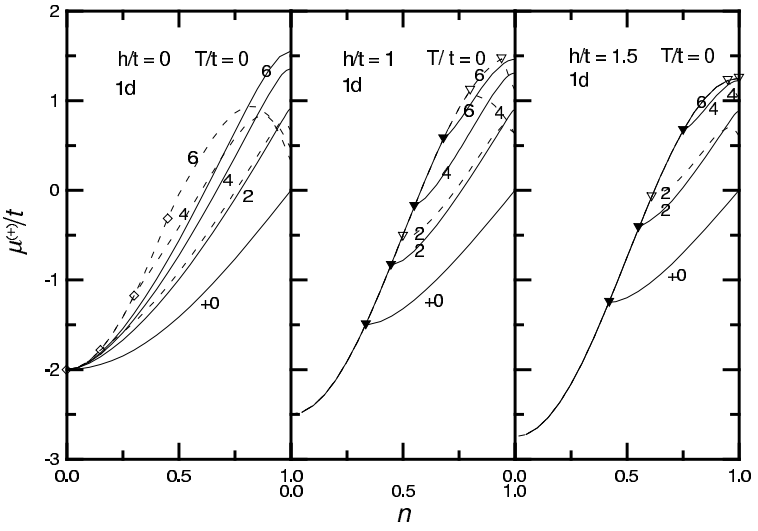

Fig. 8. $\mu^{(+)}$ as a function of n for various U/t and h/t. The notation is the same as for figure 1.

$h = 0$ we find $\mu^{(+)} \to 0$, while $\mu \to 2t$ is finite. Thus at $n = 1$ and large U/t, $\mu^{(+)}$ underestimates electron correlations and differs significantly from the exact result (figure 7). Analogous non-monotonous behavior $\mu^{(+)}$ *versus* n also takes place at intermediate U/t near $n = 1$ (figure 8).

The non-monotonous behavior of $\mu^{(+)}$ *versus* n, observed within the universal GSCF theory in 1d case (figure 7), is a signature of electron instability known also in higher dimensions.[4,36,39,20,40_42] This instability from incommensurate state into the phase-separated phase in the Hubbard model is similar to observed in the doped manganites by treating with the Kondo lattice (s-d model).[4] There are also considerable amount of experimental data pointing on a presence of a stable phase separation regime in doped cuprates,[1,3] which also contain quasi-hole rich ferromagnetic and quasi-hole free antiferromagnetic separated phases.[39]

While both antiferromagnetic and ferromagnetic states at least correspond to a local minima in an energy, a spiral phase near $n = 1$ is absolutely unstable. The most energetically favorable state corresponds to ferromagnetic metallic states embedded into the matrix of antiferromagnetic dielectric.[4,39,40_42] Within the GSCF theory the magnetic field noticeably shrinks the region of electron instability phase with negative compressibility $\kappa_{\rm ch}^{(+)} \equiv \partial\mu/\partial n < 0$ and shifts the maximum to the right, closer to $n = 1$ (figure 8). Notice that the electron instability at $h = 0$ in figure 8 takes place in the spiral phase far from transverse spin saturation (rhombuses). Such behavior is also in agree with the experimental observation that the manganites are being in separated phase only if the magnetic moment is unsaturated.[4] Thus according to the GSCF theory the phase separation in ferro- and antiferromagnetic states can be strongly suppressed by applied magnetic field.

4.4. *Double occupancy*

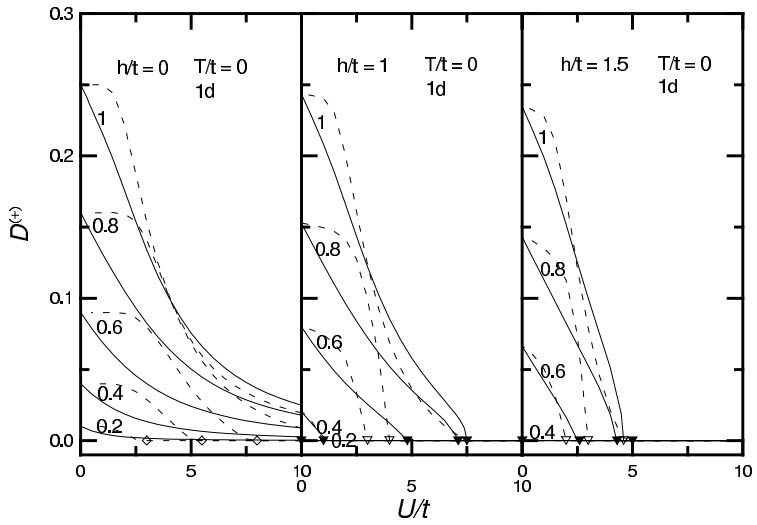

Fig. 9. The ground state concentration of doubly occupied sites $D^{(+)}$ as a function of U/t for various n and h/t. The notation is the same as for figure 1.

The exact D (Appendix C) and GSCF $D^{(+)}$ (5) are compared[35,50] in figure 9 and we see that the GSCF approach becomes ineffective at weak and intermediate interaction U/t. Though D and $D^{(+)}$ at $U/t \to 0$ both are the same, $D^{(+)}$ (the dashed curves in figure 9) barely change at weak and intermediate interaction, while the exact D (the solid curves) shows a strict linear dependence.

At large U/t the parameter $D^{(+)}$ overestimates electron correlations and decreases more rapidly than D in the exact theory. At $h = 0$ the exact result gradually approaches to the zero as U/t increases, while $D^{(+)}$ vanishes beyond the critical value $U_{\rm homog}/t$ (rhombuses) at the transition to the "transverse ferromagnetic" phase ($q = 0$) at $n \neq 1$. At $h \neq 0$, as in the exact theory, $D^{(+)}$ vanishes at $U \geq U_{\rm sat}$. Also D and $D^{(+)}$ both at fixed n are monotonous functions of U/t and h. However, in contrast to exact D a variation of $D^{(+)}$ *versus* n in general is non-monotonic.

4.5. *Phase diagram*

The Bethe-*ansatz* ground state at $h = 0$ is a singlet irrespective of n,[25,44] while the GSCF theory at large U/t shows the tendency toward the Nagaoka-like transverse ferromagnetism (spatial homogeneous phase) for all $n \neq 1$ and $h = 0$ (section 3.3).

In the spiral phase the longitudinal spin is non-saturated ($s < n/2$). However, at sufficiently large $U \geq U_{\rm sat}$, the system at $h \neq 0$ in figure 1 undergoes a transition into $s = n/2$ and $s_{j\perp} = |\Delta_q^{(+)}|/2U = 0$ with q arbitrary (degeneracy)(see section 3.1).

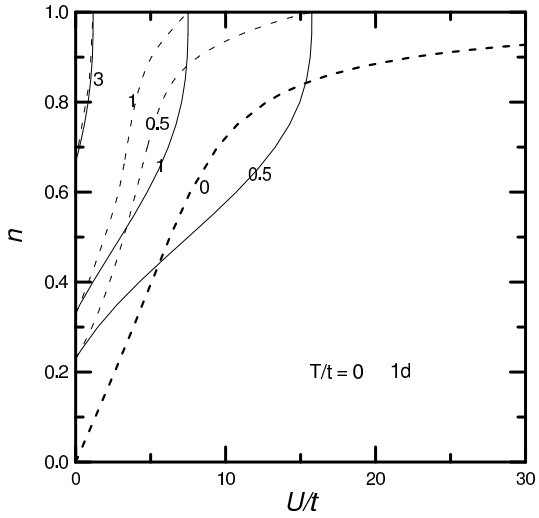

Fig. 10. The phase diagram in the U-n plan for various h/t (figures label the curves) in the Bethe-*ansatz* (the solid curves) and GSCF (the thin dashed curves) approaches. On the right of these curves we have the saturated "longitudinal ferromagnetic" phase with $s = n/2$, $\Delta_q^{(+)} = 0$ (q is arbitrary) at the corresponding $h/t > 0$, on the left we have the "transverse spiral incommensurate" phase with $q \neq 0$, $s < n/2$, $\Delta_q^{(+)} \neq 0$. The thick dashed curve corresponds to the boundary between the "transverse spiral incommensurate" phase with $s = 0$ and the spatially homogeneous "transverse ferromagnetic" phase (on the right of the curve) with the GSCF $\Delta_q^{(+)} = Un$, $q = 0$ and $s = 0$. At infinitesimal h/t the thin dashed curve coincides with the thick dashed one.

In the presence of infinitesimal magnetic field this degeneracy results in a sharp transition (spin reorientation) from saturated transverse $s_{j\perp} = n/2$ ($s = 0$) into fully polarized longitudinal $s = n/2$ ($s_{j\perp} = 0$) phase.

The U-n phase diagram at given h/t is shown in figure 10. The thick dotted curve ($h = 0$) divides the entire U-n plane on two parts with $q > 0$ (the left upper part) and $q = 0$ (the right lower part).

From self-consistent equations (12)–(14) and (15) at $h = 0$ and $q \to 0$ we find in U-n plane the equation of the phase boundary curve $U_{\rm homog}$ *versus* n between the spiral and homogeneous (ferromagnetic) phases

$$U_{\rm homog} = 2\pi t \left(\frac{1}{\sin(n\pi)} - \frac{\cos(n\pi)}{n\pi} \right). \tag{30}$$

Below the curve $U_{\rm homog}$ *versus* n we have the homogeneous (transverse ferromagnetic) state (at $h = 0$) or saturated longitudinal spin state (at $h \neq 0$). The spatial homogeneity at $h = 0$ prevails at large U/t and small n, while the spiral phase dominates at weak interaction and in close vicinity of $n = 1$.

In contrast to the exact theory the GSCF phase diagram at $h = 0$ consists exclusively of spatially ordered magnetic phases and is similar to 2d case at $n \neq 1$,[36] where incommensurate phase in 2d case eventually loses its stability to the

paramagnetic phase at $U/t \leq 1$ [38]. It is interesting that the GSCF phase diagram for the Hubbard model is similar to that for 1d Kondo model at $h = 0$.[53,54] In fact the equation (30) is close to the corresponding boundary between ferromagnetic and spiral phases in 1d Kondo model with renormalized parameter $J_c = 2U_{\rm homog}\pi n$.[52,53]

In the Bethe-*ansatz* approach the critical magnetic field $h_{\rm sat}$ of phase transition is given by the formula ($U \geq 0$) [32,35,50]

$$h_{\rm sat} = U\left(-n + \frac{\gamma}{2}\right) - \frac{U\gamma}{\pi}\arctan\left(\frac{1}{\gamma\tan n\pi}\right) - \frac{4\theta t\cos n\pi}{\pi}, \tag{31}$$

where $\gamma = \sqrt{16t^2+U^2}/U$, $\theta = \arctan(4t\sin n\pi/U)$. Particularly, at $U \to 0$ we have (23) and at $U/t \to \infty$ we have $h_{\rm sat} \to 0$ for all n.

From (31) we can see that the exact $h_{\rm sat}$ decreases with U/t for all n and increases with n for all U/t. At $n < 1$ in the GSCF approach $h_{\rm sat} = 0$ at sufficiently large but finite U/t value, which implies that the longitudinal spin saturation may occur at infinitesimal $h \to 0$, due to the degeneracy mentioned above in this section.

5. Spin crossover at half-filling

5.1. *Longitudinal spin saturation*

The lower branch ($\lambda = 1$) of the two quasi-particle energy sub-bands (9) at $n = 1$ for arbitrary h and $U \neq 0$ are separated by the finite energy gap $2\min\{E^{(+)}_{\mathbf{k}}(\pi)\}$ (see section 4.1)

At sufficiently large U/t and $h > 0$ we have the state of saturated longitudinal spin (26) (see also section 4.5). From (9) we obtain the quasi-particles energy spectrum with $\Delta^{(+)}_{\pi} = 0$

$$\mathcal{E}^{(+)}_{\mathbf{k}\lambda}(\pi) = \frac{U - \lambda|4t\cos k + U + h|}{2} \tag{32}$$

($\lambda = \pm 1$). The maximal energy of quasi-particles in the occupied band occurs at $k = \pm\pi$ (or $k_{\rm F2} = -k_{\rm F1} = \pi$).

The GSCF critical magnetic field coincides with the exact one at $n = 1$, $h_{\rm sat} = -U + \sqrt{16t^2+U^2}$.[29,58] Particularly, if $h \geq 4t$ the longitudinal spin is always saturated independently of U/t. Above $h_{\rm sat}$ or $U_{\rm sat}$, the energy gap $E^{(+)}_{\rm gap} = U + h - 4t$ increases linearly with h and U/t.

5.2. *Transverse local spin*

At $h < h_{\rm sat}$ or $U < U_{\rm sat}$ the spin s is unsaturated ($s < n/2$) and the transverse local spin $S_\perp = |\Delta^{(+)}_q|/2U$ is not zero.

The evolution of the energy gap in the momentum space with U/t and h is examined below within the GSCF approach. From (9) we find that until $2sU + h \geq 4t$ the GSCF minimum energy gap occurs at momentum $k_0 = \pi$. For opposite extreme $2sU + h < 4t$ the location of the minimum energy gap of quasi-particles occurs at

$k_0 = 0$ and in general k_0 changes according to

$$k_0 = \begin{cases} \pi & \text{if} \quad 2sU + h \geq 4t \\ \arccos\left(-(2sU + h)/4t\right) & \text{if} \quad 2sU + h < 4t, \end{cases} \tag{33}$$

and corresponding energy gap is

$$E_{\rm gap}^{(+)} = \begin{cases} \sqrt{(2sU + h - 4t)^2 + (\Delta_\pi^{(+)})^2} & \text{if} \quad 2sU + h \geq 4t \\ |\Delta_\pi^{(+)}| & \text{if} \quad 2sU + h < 4t \end{cases} \tag{34}$$

(figure 11). In particular, at $h = 0$, $s = 0$ the two sub-bands are separated by $\Delta_\pi^{(+)}$ at $k_0 = \pi/2$. This result implicitly assumes that k_0 and $q = W_{\rm Fermi}$ at $n = 1$ and $h = 0$ are both unrenormalized by U/t as in the exact theory.[36,55_57]

It is also from (33) clear that k_0 within the GSCF approach is renormalized by U/t, whenever $h \neq 0$. Earlier we studied the crossover from the itinerant BCS state into the Bose condensation regime within the attractive Hubbard model with $h = 0$.[34] Now we notice analogous crossover for $U > 0$ case at $n = 1$ and $h \neq 0$. The momentum k_0 at $h \neq 0$ increases from $k_0 < \pi$ to $k_0 = \pi$ driven by U/t. Such a weak singular behavior of the energy gap gives rise to the crossover from itinerant into the localized magnetic regime.[45] The critical magnetic field $h_{\rm cross}$ for spin crossover is determined from (33)

$$h_{\rm cross} = 4t - 2sU. \tag{35}$$

It can be shown that $h_{\rm cross} \leq h_{\rm sat}$. Thus the spin crossover always occurs in the phase of non-zero transverse spin ($S_\perp \neq 0$) with non-saturated longitudinal spin ($s < 1/2$). Analogously, at given $h \leq 4t$ from (33) (or from (35)) we have the critical interaction strength $U_{\rm cross} = (4t - h)/2s$. The formula (34) is illustrated in figure 11. We see that $E_{\rm gap}^{(+)}$ coincides with $\Delta_\pi^{(+)}$ only at $U \leq U_{\rm cross}$ (on the left of the circles in figure 11).

At $h = 0$ the gap $E_{\rm gap}$ is identical to the order parameter $\Delta_\pi^{(+)}$ and both increase with U/t. However, at $h \neq 0$ the energy gap becomes distinct from $\Delta_\pi^{(+)}$, when $E_{\rm gap}^{(+)}/t$ *versus* U/t intersects the boundary of magnetic crossover (bold curve). Apparently $\Delta_\pi^{(+)}/t$ *versus* U/t in figure 11 is non-monotonous and vanishes at magnetic saturation $U_{\rm sat}$ while $E_{\rm gap}^{(+)}/t$ monotonously increases with U/t. The curve $E_{\rm gap}^{(+)}/t$ *versus* U/t is linear above $U_{\rm sat}$ and identical to the exact gap.

The exact gap increases with U/t and h,[35] while the GSCF gap increases with U/t and is a non-monotonous function of h.[45] Although the GSCF theory overestimates the exact gap everywhere, it still correctly displays the separation between the spin ($\Delta_\pi^{(+)}$) and charge ($E_{\rm gap}^{(+)}$) degrees of freedom for $h_{\rm cross} \leq h \leq h_{\rm sat}$.

6. Summary

In the present paper we analyze the quasi-particle spectrum, the ground-state properties and the phase diagram for general U/t, n and h by employing the Bethe-*ansatz* and the GSCF approaches. The analytical GSCF theory under the extreme conditions of one dimensionality still captures the most relevant features of electron

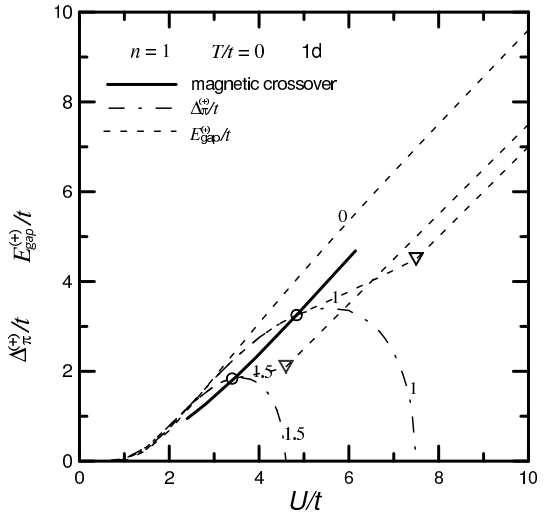

Fig. 11. The GSCF ground state energy gap $E_{\rm gap}^{(+)}/t$ (the thin dashed curves) and the order parameter $\Delta_\pi^{(+)}/t$ (the thin dash-dotted curves) *versus* U/t for $n = 1$ and various h/t (figures label the curves). The thick solid curve and the circles correspond the spin (magnetic) crossover. The triangles mark the longitudinal spin saturation. The circles mark the spin crossover.

correlations and shows in certain range of parameters also quantitative agreement with the exact result.

The GSCF ground-state properties with magnetic field always become closer to the corresponding exact results. In certain range of parameters the GSCF approach gives stable long-range ferro-, antiferro- and spiral phases with $S_\perp \neq 0$ even at $h = 0$, while the exact solution is non-magnetic (singlet) with short-range correlations.[29,36]

In contrast to the exact theory, the GSCF chemical potential $\mu^{(+)}$ in some range of U/t and n is non-monotonous, which indicates the instability of the GSCF solution with uniform electron distribution.[36,20,39_42] By comparison with the Bethe-*ansatz* solution we find that in wide range of parameters $\mu^{(+)}$ *versus* U overestimates electron correlations at $n \neq 1$ and underestimates correlations at $n = 1$. The largest absolute deviation occurs for $n = 1$ at large U/t and $h = 0$. In fact as $U/t \to \infty$, the Bethe-*ansatz* gives $\mu \to 2t$, while $\mu^{(+)} \to 0$.

The GSCF theory provides a simple relationship for the double occupancy $D^{(+)}$ in terms of parameters n, s and $\Delta_q^{(+)}$. The GSCF $D^{(+)}$ underestimates electron correlations at weak interaction and overestimates at large U/t. At $h = 0$ the GSCF $D^{(+)}$ vanishes at large U/t, while exact D decreases gradually as U/t increases.

Exactly at $n = 1$ and $h \neq 0$ the GSCF theory even in 1d case displays the spin-charge separation, where antiferromagnetic order parameter $\Delta_\pi^{(+)}$ differs from the electron-hole excitation gap $E_{\rm gap}^{(+)}$. This in turn gives rise to a smooth magnetic crossover from the itinerant weak band-like moment to the localized magnetism of Bose condensed electron-hole pairs with well developed moment.

The GSCF variational ground state energy is exact in limiting cases $U/t \to 0$ and $U/t \to \infty$ for arbitrary $h \geq 0$ and all $0 \leq n \leq 1$. By choosing single-particle mean field Hamiltonian as a zero order approximation we can construct a nontrivial perturbation expansion procedure, which converges for arbitrary perturbation parameter.[24] We find that a variational calculation gives us the first two terms of the expansion series, in which the perturbation potential is equal to the deviation between the Hubbard and GSCF Hamiltonian. Corresponding second order corrections to the ground state energy vanish at small and large U/t limits and provide good numerical agreement with the Bethe-*ansatz* result in wide range of parameters.

Acknowledgments

One of us (ANK) grateful to Steven A. Kivelson and Jim Allen for stimulating discussions. The research was supported by the National Science Council of Taiwan (under Grants NSC 91-2112-M-032-016 and NSC 90-2112-M-034-002).

References

1. P. W. Anderson, *Physics Today* **6** 54-61 (1991)
2. V. J. Emery and S. A. Kivelson, *Nature* **374** 434-437 (1995).
3. J. D. Denlinger, G. -H. Gweon, J. W. Allen, *Phys. Rev. Lett.* **82** 2540-2543 (1999), G. -H. Gweon, J. D. Denlinger, J. W. Allen *ibid* **85** 3985-3985, (2000); J. W. Allen and et al. *The Hubbard Model*, Plenum Press, Edited by Baeriswyl et al. (1995) 357.
4. E. L. Nagaev, *Sov. Physics-Uspekhi* **38** 497-520 (1995),
5. Yu. Irkhin and M. I. Katsnel'son, *Sov. Physics-Uspekhi* **37** 659-676 (1994).
6. R. Weht, W. E. Pickett, *Phys. Rev.* B **60** 13006-13010 (1999).
7. L. P. Gorkov, *Sov. Phys.-Usp.* **27** 809-829 (1984).
8. J. Wosnitza *Fermi Surfaces of Low-Dimensional Organic Metals and Superconductors* (Berlin: Springer-Verlag, 1996).
9. N. Dupuis and G. Montambaux, *Phys. Rev.* B **49** 8993-9008 (1994).
10. P. Nozieres, *Eur. Phys. J.* **B** 10 649-662 (1999).
11. D. R. Penn, *Phys. Rev.* **142** 350-365 (1966).
12. D. I. Khomskii, *Fiz. Metal. Metalloved.* **29** 31-57 (1970)
13. W. D. Langer, M. Plischke and D. C. Mattis, *Phys. Rev. Lett.* **23** 1448–1452 (1969).
14. W. D. Langer and D. C. Mattis, *Phys. Lett.* **36A** 139-140 (1971).
15. G. Kotliar and A. E. Ruckenstein, *Phys. Rev. Lett.* **57** 1362-1365 (1986).
16. M. R. Hedayati, and G. Vignale, *Phys. Rev.* **B40**, 9044 (1993).
17. J. E. Hirsch, *Phys. Rev.* B **31** 4403-4419 (1985).
18. E. Dagotto, *Rev. Mod. Phys.* **66** 763-840 (1994).
19. Y. Nagaoka, *Phys. Rev.* **147** 392-405 1966).
20. E. Eisenberg, R. Berkovits, D. A. Huse and B. L. Altshuler, *Phys. Rev.* **B 65** 134437-1 - 134437-7 (2002).
21. P. Nozeres and S. Schmitt-Rink, *J. Low Temp. Phys.* **59** 195-211 (1985).
22. J. R. Schrieffer, X. G. Wen and S. C. Zhang, *Phys. Rev.* B **39** 11663-11679 (1989).
23. *The Hubbard Model Its Physics and Mathematical Physics*, edited by D.B. Baeriswyl et al., **343** pp. 117-225 (NATO ASI Series: Plenum Press, New York 1995).
24. A. N. Kocharian, C. Yang and Y. L. Chiang, *Int. J. Mod. Phys.* B in press (2003).
25. E. H. Lieb and F. Y. Wu, *Phys. Rev. Lett.* **20** 1445-1448 (1968), E. H. Lieb and F. Y. Wu, *Phys. Rev. Lett.* **21** 192-192 (1968).

26. M. Takahashi, *Progr. Theor. Phys.* **42** 1098-1105 (1969), *ibid*, **44** 348 (1970); *ibid* **43** 1619 (1970).
27. D. C. Mattis, The Many-Body Problem: An Encyclopedia of Exactly Solved Models in One Dimension, ed. by Daniel C. Mattis (World Scientific, 1994).
28. H. Shiba, *Phys. Rev.* B **6** 930-938 (1972).
29. H. Frahm and V. E. Korepin, *Phys. Rev.* B **42** 10553-10565 (1990), H. Frahm and V. E. Korepin, *Phys. Rev.* B **43** 5653-5662 (1990).
30. P. Schlottmann, *Int. J. Mod. Phys.* **B 11** 355-667 (1997).
31. N. Kawakami and A. Okiji, *Progr. Theor. Phys. Supplement* **101** 429-440 (1990), N. Kawakami, T. Usuki and A. Okiji, *Phys. Lett* A **137** 287-290 (1989).
32. J. Carmelo, P. Horsh, P. A. Bares, and A. A. Ovchinnikov *Phys. Rev.* B **44** 9967-9980 (1991).
33. T. Deguchi, F. H. L. Essler, F. Göhmann, A. Klüpper, V. A. Korepin, K. Kusakabe K, *Physics Reports* **331** 197-281 (2000).
34. A. N. Kocharian, C. Yang and Y. L. Chiang, *Phys. Rev.* B **59** 7458-7472 (1999), *Int. J. Mod. Phys.* B **29-31** 3538-3545 (2001); *Physica* C **364-365** 131-133 (1999).
35. C. Yang, A. N. Kocharian and Y. L. Chiang, *J Phys.: Condens. Matter* B **12** 7433-7454 (2000), *Physica* C **341-348** 245-246 (2000).
36. H. J. Schulz, *Phys. Rev. Lett* **65** 2462-2465 (1990), *ibid* **64** 2831-2834 (1990), *ibid* **64** 1445-1448 (1990).
37. H. R. Krishnamurthy, C. Jayaprakash, S. Sarker and W. Wenzel, *Phys. Rev. Lett.* **64** 950-953 (1976).
38. S. Sarker, C. Jayaprakash, H. R. Krishnamurthy and W. Wenzel, 1991 *Phys. Rev.* B **43** 8775-8778 (1991), C. Jayaprakash, H. R. Krishnamurthy, and S. Sarke, *Phys. Rev.* B **40** 2610-2613 (1989).
39. V. J. Emery, S. A. Kivelson and H. Q. Lin *Phys. Rev. Lett.* **64** 475-478 (1990).
40. A. M. Tsvelik, *Quantum Field Theory in Condensed Matter Physics* (Cambridge University Press, 1995) p 275.
41. T. Hanish and E. Muller-Hartmann, *Ann. Phys., Lpz* **2** 381-397 (1993).
42. P. B. Visscher, *Phys. Rev.* B **10** 943-945 (1974).
43. G. W. Fernando, A. N. Kocharian, R. E. Watson and M. Weinert, *Physica* B **230-232** 509-512 (1997).
44. L. E. Lieb and D. C. Mattis, *Phys. Rev.* **125** 164-172 (1962).
45. A. N. Kocharian, N. Kioussis and S. Park, *J. Phys.: Condens. Matter* **13** 6759-6772 (2001).
46. Ballentine L E 1990 *Quantum Mechanics* (New Jersey: Prentice-Hall International Editions)
47. D. C. Mattis, *Revs. Mod. Phys.*, **58** 361 (1986).
48. A. N. Kocharian and A. S. Saakyan, *Phys. Solid State* **40** 336-340 (1998).
49. W. H. Press, *Numerical Recipes in Fortran* 2nd ed (New York: Cambridge University Press, 1992)
50. Y. L. Chiang, Ph.D. Thesis, Tamkang University, Tamsui, Taiwan, 2000.
51. P. Nozieres, *Eur. Phys. J.* **B** 6, 447-457 (1998).
52. P. Fazekas and E. Muller-Hartmann, *Z. Phys.* B **85** 285 (1991).
53. H. Tsunetsugu, M. Sigrist and K. Ueda, *Rev. Mod. Phys.* **69** 819-821 (1997).
54. J. E. Hirsch, *Phys. Rev.* **B 30** 5383-5385 (1984).
55. K. B. Blagoev and K. S. Bedell, *Phys. Rev. Lett.* **79** 1106-1109 (1997).
56. M. Yamanaka, M. Oshikawa and I. Affleck, *Phys. Rev. Lett.* **79** 1110-1113 (1997).
57. H. Shiba and M. Ogata, *Prog. Theor. Phys. Supplement* **108** 265-286 (1992), H. Shiba, Sugiyama and M. Ogata, *Phys. Rev.* B **43** 8401-8410 (1991).

58. A. N. Kocharian and J. Sebold J, *Phys. Rev.* B **53** 12804-12812 (1996).

Appendix A. The GSCF wave number at weak interaction

We consider the GSCF approach at weak interaction limit for $U \to +0$ at $h = 0$ and $0 \leq n \leq 1$. In this limit: $\Delta_q^{(+)} \to 0$, $s = 0$. The formula (11) reduces simply to

$$E_k^{(+)}(q) = \frac{|\epsilon_k - \epsilon_{k+q}|}{2} \tag{A.1}$$

and from (9) we have

$$\mathcal{E}_{k+}^{(+)}(q) = \epsilon_{k+q}, \qquad \mathcal{E}_{k-}^{(+)}(q) = \epsilon_k, \qquad (\text{if } \epsilon_k > \epsilon_{k+q}), \tag{A.2}$$

$$\mathcal{E}_{k+}^{(+)}(q) = \epsilon_k, \qquad \mathcal{E}_{k-}^{(+)}(q) = \epsilon_{k+q}, \qquad (\text{if } \epsilon_k < \epsilon_{k+q}). \tag{A.3}$$

In the ground state the quasi-particle states $\{k,-\}$ are all empty, and the states $\{k,+\}$ are partially (if $n < 1$) or entirely (if $n = 1$) occupied in momentum space at $k_{\rm F1} \leq k \leq k_{\rm F2}$ with $k_{\rm F2} - k_{\rm F1} = 2n\pi$. In order to satisfy the equation (12), $k_{\rm F1}$ and $k_{\rm F2}$ must be disposed symmetrically with respect to the point of intersection k_0 of the functions ϵ_k and ϵ_{k+q}:

$$\epsilon_{k_0} = \epsilon_{k_0+q}, \qquad k_0 = \frac{k_{\rm F1} + k_{\rm F2}}{2}. \tag{A.4}$$

Hence we obtain $k_{\rm F1} = k_0 - n\pi$, $k_{\rm F2} = k_0 + n\pi$. Besides, we must have

$$\mathcal{E}_{k_{\rm F1}+q\,+}^{(+)}(q) = \mathcal{E}_{k_{\rm F2}\,+}^{(+)}(q) = \mathcal{E}_{k_0\,+}^{(+)}(q) = E_{\rm F}, \tag{A.5}$$

where $E_{\rm F}$ is the Fermi energy, or $\epsilon_{k_{\rm F1}+q} = \epsilon_{k_{\rm F2}} = \epsilon_{k_0}$. From (A.5) we obtain the final result for q:

$$q = n\pi. \tag{A.6}$$

Note, that the equation (13) is satisfied, since $\Delta_q^{(+)} \to 0$. It is not difficult to see that the equation (14) is also satisfied. The relationship (A.6) is in agreement with the Luttinger theorem for the corresponding lattice momentum in the spin-spin correlation function.[36,55_57]

Appendix B. Ground state energy and chemical potential in the exact theory

The Bethe-*ansatz* technique [25] (see also [34,35,50]) gives an exact expression for the ground state energy of the Hubbard model in one dimension:

$$E = -2t \int_{-Q}^{Q} dk \rho(k) \cos k, \tag{B.1}$$

where $0 \leq n \leq 1$, $0 \leq s \leq n/2$, $\rho(k)$ is determined from the set of coupled Fredholm integral equations

$$\rho(k) = \frac{1}{2\pi} + \frac{U \cos k}{4t\pi} \int_{-B}^{B} d\lambda \sigma(\lambda) f_1(k,\lambda), \tag{B.2}$$

$$\sigma(\lambda) = \frac{U}{4t\pi}\int_{-Q}^{Q} dk\rho(k) f_1(k,\lambda) - \frac{U}{2t\pi}\int_{-B}^{B} d\lambda'\sigma(\lambda') f_2(\lambda,\lambda') , \tag{B.3}$$

$$f_1(k,\lambda) \equiv \frac{1}{(U/4t)^2 + (\lambda - \sin k)^2} , \tag{B.4}$$

$$f_2(\lambda,\lambda') \equiv \frac{1}{(U/2t)^2 + (\lambda - \lambda')^2} , \tag{B.5}$$

with normalization conditions determining Q and B

$$\int_{-Q}^{Q} \rho(k)dk = n, \tag{B.6}$$

$$\int_{-B}^{B} \sigma(\lambda)d\lambda = \frac{n}{2} - s . \tag{B.7}$$

In the exact theory from $\mu = \partial E/\partial n$ and (B.1)– (B.7) we have for the chemical potential

$$\mu = -2t\int_{-Q}^{Q} dk\rho_n(k)\cos k - 4tQ_n\rho(Q)\cos Q, \tag{B.8}$$

where $\rho_n(k) \equiv \partial\rho(k)/\partial n$ and $\sigma_n(\lambda) \equiv \partial\sigma(\lambda)/\partial n$ satisfy the integral equations

$$\begin{aligned}\rho_n(k) = & \frac{U\cos k}{4t\pi}\int_{-B}^{B} d\lambda\sigma_n(\lambda) f_1(k,\lambda) \\ & + \frac{U\cos k}{4t\pi}\left[f_1(k,B) + f_1(k,-B)\right]\sigma(B) B_n ,\end{aligned} \tag{B.9}$$

$$\begin{aligned}\sigma_n(\lambda) = & \frac{U}{4t\pi}\int_{-Q}^{Q} dk\rho_n(k) f_1(k,\lambda) - \frac{U}{2t\pi}\int_{-B}^{B} d\lambda'\sigma_n(\lambda') f_2(\lambda,\lambda') \\ & + \frac{U}{4t\pi}\left[f_1(Q,\lambda) + f_1(-Q,\lambda)\right]\rho(Q) Q_n \\ & - \frac{U}{2t\pi}\left[f_2(\lambda,B) + f_2(\lambda,-B)\right]\sigma(B) B_n ,\end{aligned} \tag{B.10}$$

and $Q_n \equiv \partial Q/\partial n$, $B_n \equiv \partial B/\partial n$ are determined from the relations

$$\int_{-Q}^{Q} \rho_n(k)\, dk + 2\rho(Q) Q_n = 1, \tag{B.11}$$

$$\int_{-B}^{B} \sigma_n(\lambda)d\lambda + 2\sigma(B) B_n = \frac{1}{2} . \tag{B.12}$$

Eqs. (B.8)–(B.12) with (B.2)–(B.7) determine μ as a function of U/t, n and s.

Appendix C. Double occupancy in the exact theory

In the exact theory from $D = \partial E/\partial U$ and (B.1)– (B.7) we have[34,35,50]

$$D = -2\int_{-Q}^{Q} dk\rho_U(k)\cos k - 4\rho(Q)\,Q_U\cos Q\ , \tag{C.1}$$

where $\rho_U(k) \equiv t\partial\rho(k)/\partial U$ and $\sigma_U(\lambda) \equiv t\partial\sigma(\lambda)/\partial U$ satisfy the integral equations

$$\begin{aligned}\rho_U(k) = {} & \frac{U\cos k}{4t\pi}\int_{-B}^{B} d\lambda\sigma_U(\lambda) f_1(k,\lambda) \\ & + \frac{\cos k}{2\pi}\int_{-B}^{B} d\lambda\sigma(\lambda)\left[f_1(k,\lambda)/2 - (U/4t)^2 f_1(k,\lambda)^2\right] \\ & + \frac{U\cos k}{4t\pi}\left[f_1(k,B) + f_1(k,-B)\right]\sigma(B)\,B_U,\end{aligned} \tag{C.2}$$

$$\begin{aligned}\sigma_U(\lambda) = {} & \frac{U}{4t\pi}\int_{-Q}^{Q} dk\rho_U(k) f_1(k,\lambda) - \frac{U}{2t\pi}\int_{-B}^{B} d\lambda'\sigma_U(\lambda') f_2(\lambda,\lambda') \\ & + \frac{U}{2U\pi}\int_{-Q}^{Q} dk\rho(k)\left[f_1(k,\lambda)/2 - (U/4t)^2 f_1(k,\lambda)^2\right] \\ & - \frac{U}{U\pi}\int_{-B}^{B} d\lambda'\sigma(\lambda')\left[f_2(\lambda,\lambda')/2 - (U/2t)^2 f_2(\lambda,\lambda')^2\right] \\ & + \frac{U}{4t\pi}\left[f_1(Q,\lambda) + f_1(-Q,\lambda)\right]\rho(Q)\,Q_U \\ & - \frac{U}{2t\pi}\left[f_2(\lambda,B) + f_2(\lambda,-B)\right]\sigma(B)\,B_U,\end{aligned} \tag{C.3}$$

and $Q_U \equiv t\partial Q/\partial U$, $B_U = t\partial B/\partial U$ are determined from

$$\int_{-Q}^{Q}\rho_U(k)dk + 2\rho(Q)\,Q_U = 0, \tag{C.4}$$

$$\int_{-B}^{B}\sigma_U(\lambda)d\lambda + 2\sigma(B)\,B_U = 0. \tag{C.5}$$

The functions $f_1(k,\lambda)$ and $f_2(\lambda,\lambda')$ are defined by (B.4), (B.5).

Substituting the solution of the integral Bethe-*ansatz* equations (B.1)–(B.7) into (C.2)–(C.5) and resolving these equations we obtain D as a function of U/t, n and s.